Available online at www.sciencedirect.com
SCIENCE DIRECT
Journal of Molecular Catalysis A: Chemical 246 (2006) 176–184
JOURNAL OF MOLECULAR CATALYSIS A: CHEMICAL
www.elsevier.com/locate/molcata

Preparation, characterization and photocatalytic activity of in situ N,S-codoped TiO_2 powders

Jiaguo Yu [a,*], Minghua Zhou [a,b], Bei Cheng [a], Xiujian Zhao [a]

[a] *State Key Laboratory of Advanced Technology for Material Synthesis and Processing, Wuhan University of Technology, Wuhan 430070, PR China*
[b] *Staff Room of Chemistry, Yunyang Medical College, Shiyan 442000, Hubei, PR China*

Received 7 October 2005; received in revised form 26 October 2005; accepted 26 October 2005
Available online 5 December 2005

Abstract

A simple method for preparing highly photoactive nanocrystalline mesoporous N,S-codoped TiO_2 powders was developed by hydrolysis of $Ti(SO_4)_2$ in a $NH_3{\cdot}H_2O$ solution at room temperature. The as-prepared TiO_2 powders were characterized with X-ray diffraction (XRD), X-ray photoelectron spectroscopy (XPS), thermalgravimetric and differential thermal analysis (TG–DTA), UV–vis diffuse reflectance spectra, N_2 adsorption–desorption measurements, scanning electron microscope (SEM) and transmission electron microscopy (TEM). The photocatalytic activity was evaluated for the photocatalytic oxidation of acetone and formaldehyde under UV light and daylight irradiation in air, respectively. The results showed that the as-prepared TiO_2 powders exhibited a stronger absorption in the UV–vis light region and a red shift in the band gap transition due to N,S-codoping. The photocatalytic activity of the as-prepared N,S-codoped TiO_2 powders at a temperature range of 400–700 °C were obviously higher than that of commercial Degussa P25. Especially, the daylight-induced photocatalytic activities of the as-prepared N,S-codoped TiO_2 powders were about ten times greater than that of Degussa P25. The high activities of the N,S-codoped TiO_2 can be attributed to the results of the synergetic effects of strong absorption in the UV–vis light region, red shift in adsorption edge, good crystallization, large surface area and two phase structures of undoped TiO_2 and N,S-codoped TiO_2.

Keywords: Photocatalytic activity; N,S-codoping; TiO_2; Daylight-induced; Nanocrystalline; Mesoporous

1. Introduction

In recent years, in order to solve the increasingly serious environmental pollution problems, heterogeneous semiconductor photocatalysis gradually becomes a popular technique for its potential to control aqueous contaminates or air pollutants. Among various oxide semiconductors, TiO_2 has been proved to be the most suitable photocatalyst for widespread environmental applications because of its biological and chemical inertness, strong oxidizing power, non-toxicity and long-term stability against photo and chemical corrosion [1–9]. However, TiO_2 can be activated only under UV light of wavelengths <387 nm irradiation due to its large band gap of 3.2 eV. The solar spectrum usually contains about 4% UV light. Therefore, the optical response of TiO_2 shifting into the visible-light region will enhance its photocatalytic activity under daylight or solar irradiation [10]. Furthermore, to reduce the recombination of photo-generated electrons and holes of TiO_2, and to extend its light absorption into the visible-light region, various metal and non-metal ions have been doped into titania [11–20]. Especially, Asahi et al. reported that the photocatalytic activity and hydrophilicity of TiO_2 could be enhanced by nitrogen doped into the substitutional sites of TiO_2 ($TiO_{2-x}N_x$) [21]. This is due to the fact that the band gap of TiO_2 can be narrowed by these elements doping, and thus make the absorption edge of TiO_2 moving to the visible-light region. Recently, Umebayashi et al. [22–24] have succeeded to synthesize S-doped TiO_2, which was used as an efficient visible-light-induced photocatalyst for visible-light photocatalytic degradation of methylene blue. They suggested that sulfur was doped as an anion and replaced the lattice oxygen in TiO_2. Ohno et al. [25–27] found that S atoms could be incorporated as cations and replaced Ti ions in the sulfur-doped TiO_2 photocatalyst. Zhao et al. [28] and Majima and co-workers [29] reported that doping TiO_2 with boron or sulfur could also

* Corresponding author.
E-mail address: jiaguoyu@yahoo.com (J. Yu).

1381-1169/$ – see front matter © 2005 Elsevier B.V. All rights reserved.
doi:10.1016/j.molcata.2005.10.034

reduce its band gap and shift its optical response to the visible-light region. Undeniably, the non-metal-element-doping of TiO_2 photocatalyst become a hot research topic, and it opens up a new possibility for the development of solar- or daylight-induced photocatalytic materials.

These non-metal elements, such as N, F, S and B, have been proved to be beneficial doping elements in the TiO_2 through mixing their p orbital with O 2p orbital to reduce the band gap energy of TiO_2 [30–41]. However, to the best of our knowledge, the effects of N,S-codoping and heat-treatment temperature on the photocatalytic activity and microstructures of nanocrystalline mesoporous TiO_2 powders prepared by a facile precipitate method using $Ti(SO_4)_2$ and $NH_3{\cdot}H_2O$ as precursors have not been reported. This work may provide new insights into the preparation of highly photoactive TiO_2 powders.

2. Experimental

2.1. Preparation

All chemicals used in this study were reagent-grade without further purification. Deionized water was used in the whole experiment. The TiO_2 powders were synthesized by hydrolysis of $Ti(SO_4)_2$ in a $NH_3{\cdot}H_2O$ aqueous solution. The aqueous solution of $Ti(SO_4)_2$ (0.5 M, 50 mL) was added drop-wise to a 100 mL $NH_3{\cdot}H_2O$ aqueous solution (1.0 M) in a 250 mL beaker under continuous stirring for 60 min. After hydrolysis reaction, the white precipitate was centrifuged, and then washed with distilled water and alcohol for five times. The obtained white gels were dried under vacuum at 80 °C for 10 h and were ground to obtain xerogel samples. The white xerogel were calcined at 400, 500, 600, 700 and 800 °C in air for 3 h, respectively.

2.2. Characterization

The crystallization behavior was monitored using a DTA–TG instrument (Netzsch STA 449C) in airflow of 100 mL min^{-1} at a heating rate of 10 °C min^{-1} from room temperature to 900 °C. The X-ray diffraction (XRD) patterns obtained on a X-ray diffractometer (type HZG41B-PC) using Cu Kα irradiation at a scan rate of 0.05° $2\theta\,s^{-1}$ were used to determine the identity of any phase present and their crystallite size. The accelerating voltage and the applied current were 15 kV and 20 mA, respectively. If the sample contains anatase and rutile phases, the mass fraction of rutile can be calculated according to Eq. (1) [11,42–44].

$$W_R = \frac{A_R}{0.886A_A + A_R} \quad (1)$$

where A_A and A_R represent the integrated intensities of the anatase (1 0 1) and rutile (1 1 0) peaks, respectively. The average crystallite sizes of anatase and rutile were determined according to the Scherrer equation using the full-width half-maximum data of each phase after correcting the instrumental broadening. The Brunauer–Emmett–Teller (BET) surface area (S_{BET}) of the powders was analyzed by nitrogen adsorption in an AUTOSORB-1 (Quantachrome Instruments, USA) nitrogen adsorption apparatus. All the calcined samples and Degussa P25 were degassed at 180 °C prior to nitrogen adsorption measurements. The BET surface area was determined by multipoint BET method using the adsorption data in the relative pressure (P/P_0) range of 0.05–0.3. Desorption isotherm was used to determine the pore size distribution via the Barret–Joyner–Halender (BJH) method with cylindrical pore size [45]. The nitrogen adsorption volume at the relative pressure (P/P_0) of 0.994 was used to determine the pore volume and average pore size. Crystallite sizes and shapes were observed using transmission electron microscopy (TEM) (JEOL 1200EX, Japan). The particle morphologies of TiO_2 powders were characterized by scanning electron microscopy (SEM) (type JSM-5610LV) with an accelerating voltage of 20 kV. X-ray photoelectron spectroscopy (XPS) measurements were done with a Kratos XSAM800 XPS system with Cu Kα source and a charge neutralizer; all the binding energies were referenced to the C 1s peak at 284.8 eV of the surface adventitious carbon. UV–vis diffused reflectance spectra of TiO_2 powders were obtained for the dry-pressed disk samples using a UV–vis spectrophotometer (UV2550, Shimadzu, Japan). $BaSO_4$ was used as a reflectance standard in a UV–vis diffuse reflectance experiment.

2.3. Measurement of photocatalytic activity

The photocatalytic activity experiments of the as-prepared TiO_2 powders and Degussa P25 for the oxidation of acetone or formaldehyde in air were performed at ambient temperature using a 15 L photocatalytic reactor [46,47]. The catalysts were prepared by coating an aqueous suspension of TiO_2 powders onto three dishes with a diameter of about 9.0 cm. The weight of catalysts used for each experiment was kept 0.3 g. The dishes containing catalysts were dried in an oven at 100 °C for about 2 h to evaporate the water and then cooled to room temperature before used. After TiO_2-coated dishes were placed in the reactor, a small amount of acetone or formaldehyde was injected into the reactor with a micro-syringe. The analysis of acetone, formaldehyde, carbon dioxide and water vapor concentration in the reactor was conducted on line with a Photoacoustic IR Multigas Monitor (INNOVA Air Tech Instruments Model 1312). The acetone or formaldehyde vapor was allowed to reach adsorption equilibrium with catalysts in the reactor prior to UV light or daylight irradiation. The initial concentration of acetone or formaldehyde after adsorption equilibrium was controlled at 350 ± 10 and 200 ± 10 ppm, respectively. Which remained constant for about 5 min until a UV or daylight lamp (6 cm above the dishes) in the reactor was turned on. Integrated UV and daylight intensity were measured with a UV radiometer (UV-A, made in Photoelectric Instrument Factory of Beijing Normal University) were 2.9 ± 0.1 mW/cm^2 (the peak intensity of 365 nm) and 0.46 ± 0.01 mW/cm^2 (the peak intensity of 420 nm), respectively. The initial temperature was 25 ± 1 °C and each set of experiment in UV and daylight illumination was performed for 60 and 180 min, respectively.

Since photocatalytic degradation of acetone or formaldehyde on the surface of mesoporous TiO_2 powders is a heterogenous reaction, which generally follows a Langmuir–Hinshelwood

mechanism [2,4,48,49] with the rate r being proportional to the coverage θ:

$$r = k\theta = \frac{kKc}{1 + Kc} \quad (2)$$

where k is the true rate constant including various parameters, such as the mass of catalyst, the intensity of ultraviolet or visible-light, etc. and K is the adsorption constant. In a heterogenous solid–gas reaction, the photocatalytic reaction of acetone or formaldehyde on the surface of TiO_2 powders is a pseudo-first order reaction and its kinetic equation may be expressed as follows:

$$r = -\frac{dc}{dt} = kKc = k_a c \quad (3)$$

where k_a is the apparent rate constant of pseudo-first order. So, the decrease of gas concentration will follow the arithmetical progression proportion. The rate equation is

$$\ln \frac{c_0}{c_t} = k_a t \quad (4)$$

Furthermore, the photocatalytic activity of the samples can also be quantitatively evaluated by comparing the removal efficiency of reactant (R(%)). R(%) was calculated according to the following equation [46]:

$$R(\%) = \frac{[\text{gas}]_0 - [\text{gas}]_t}{[\text{gas}]_0} \times 100\% \quad (5)$$

where $[\text{gas}]_0$ and $[\text{gas}]_t$ represent the initial equilibrium concentration and reaction concentration of reactant, respectively.

3. Results and discussion

3.1. Thermal analysis

Fig. 1 shows the differential thermal analysis–thermogravimetry (DTA–TG) curves of the TiO_2 xerogel powders prepared by hydrolysis of $Ti(SO_4)_2$ in a $NH_3{\cdot}H_2O$ solution at room temperature and dried under vacuum at 80 °C for 10 h. A very small endothermic peak at about 100 °C was due to the desorption of the physically adsorbed water and alcohol [50]. The relatively great exothermic peak at 270 °C probably comes from

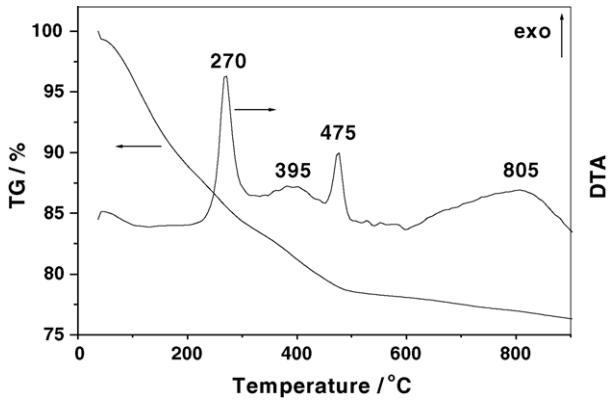

Fig. 1. DTA–TG curves of the as-prepared TiO_2 xerogel powders dried at 80 °C.

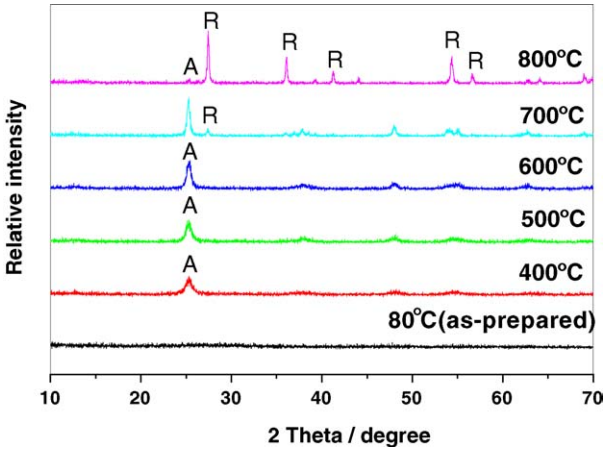

Fig. 2. XRD patterns of the as-prepared TiO_2 powders calcined at different temperatures.

the thermal decomposition of unhydrolyzed $Ti(SO_4)_2$ remained in the TiO_2 xerogel powders [11]. The DTA curve also shows two exothermic peaks at about 395 and 475 °C, respectively. The two peaks are probably caused by the phase transformation of amorphous to anatase [50,51]. Why there are two phase transformation temperatures (from amorphous to anatase) existed in the xerogel? One possible explanation is that the TiO_2 xerogel samples contain two kinds of TiO_2: doped and undoped TiO_2 (as shown in Figs. 6 and 7). The exothermic peak at 395 °C can be assigned to the phase transformation from amorphous to anatase of undoped (pure) TiO_2 in the as-prepared powders [52]. The other exothermic peak for the phase transformation from amorphous to anatase shifts to a higher temperature. This is probably ascribed to the fact that the phase transformation of the N,S-codoped TiO_2 from amorphous to anatase is suppressed by the presence of N and S elements (as shown in Fig. 6). At around 805 °C, a broad exothermic peak is observed, which can be assigned to the phase transformation from anatase to rutile (as shown in Fig. 2). It can be concluded from the DTA result that the as-prepared TiO_2 sample was amorphous. The TG curve can be roughly divided into three stages. The first stage is from room temperature to 200 °C, over which the mass loss is the greatest. A mass loss of up to 12.0% was observed, which was caused by the evaporation of the physical adsorbed water and alcohol from the xerogels [11]. The second stage is from 200 to 500 °C, where the mass loss is about 10.0%. This can be assigned to the decomposition of unhydrolyzed $Ti(SO_4)_2$ in the xerogels. The third stage is from 500 to 900 °C and the mass loss is about 4.0%, which is attributed to the removal of chemisorbed water [53].

3.2. Phase structure

XRD was used to investigate the changes of phase structure of the as-prepared TiO_2 xerogel powders before and after heat-treatment. Fig. 2 shows the effects of calcination temperature on the phase structures of TiO_2 xerogel powders. It can be seen that the calcination temperature obviously influ-

Table 1
Effects of calcination temperatures on physical properties of TiO_2 powders

Temperature (°C)	Phase content[a]	S_{BET}[b] (m^2/g)	Pore volume[c] (cm^3/g)	Average pore size[c] (nm)	Porosity[d] (%)	Crystalline size[e] (nm)
400	A	192.5	0.611	12.7	70.5	12.0(1.0)
500	A	145.2	0.507	14.0	66.4	13.6(1.3)
600	A	91.5	0.427	18.7	62.5	19.4(1.6)
700	A(81%) + R(19%)	56.1	0.342	24.4	57.2	38.2(A)(2.3)
800	A(7%) + R(93%)	14.7	0.171	46.5	40.0	68.1(R)
P25	A(80%) + R(20%)	63.0	0.060	3.8	19.0	30.0(A)

[a] A and R denote anatase and rutile, respectively.
[b] The BET surface area was determined by multipoint BET method using the adsorption data in P/P_0 range from 0.05 to 0.3.
[c] Pore volume and average pore size were determined by nitrogen adsorption volume at $P/P_0 = 0.994$.
[d] The porosity is estimated from the pore volume determined using the desorption data at $P/P_0 = 0.994$.
[e] Average crystalline size of TiO_2 was determined by XRD using Scherrer equation. Relative anatase crystallinity: the relative intensity of the diffraction peak from the anatase (1 0 1) plane (indicated in parentheses, reference = sample calcined at 400 °C).

ences the crystallization and phase composition of the TiO_2 powders. At 80 °C, the as-prepared powders were amorphous. At 400 °C, anatase phase appears. With increasing calcination temperatures (from 400 to 700 °C), the peak intensities of anatase increase and the width of the (1 0 1) plane diffraction peak of anatase ($2\theta = 25.4°$) becomes narrower, The rutile phase starts to appear at 700 °C. TiO_2 powders thus contain two different phases: anatase and rutile. The mass percentages of anatase and rutile are 81 and 19%, respectively. At 800 °C, rutile is a main phase and its content is 93% (as shown in Table 1).

The structure of TiO_2 powders was further studied by TEM image and selective area electron diffraction (SAED). Fig. 3(a) shows the TEM image and SAED pattern (inset) of the TiO_2 powders obtained at 500 °C. It can be seen that the primary particle size is about 14 ± 2 nm, which is in agreement with the value of the crystallite size determined by XRD (14.0 nm) (as shown in Table 1). The phase structure of TiO_2 at 500 °C was also confirmed to be anatase phase by SAED analysis. Fig. 3(b) shows SEM micrographs of the TiO_2 powders calcined at 500 °C. The powders are found to be fine and slightly agglomerated. Further observation indicates that the morphology of TiO_2 powders is very rough and may be beneficial to enhancing the adsorption of reactants due to its great surface roughness and high surface area.

3.3. BET surface areas and pore structure

Fig. 4 shows the nitrogen adsorption–desorption isotherms of the TiO_2 powders calcined at different temperatures. It can be seen that the N_2 adsorption–desorption isotherms of TiO_2

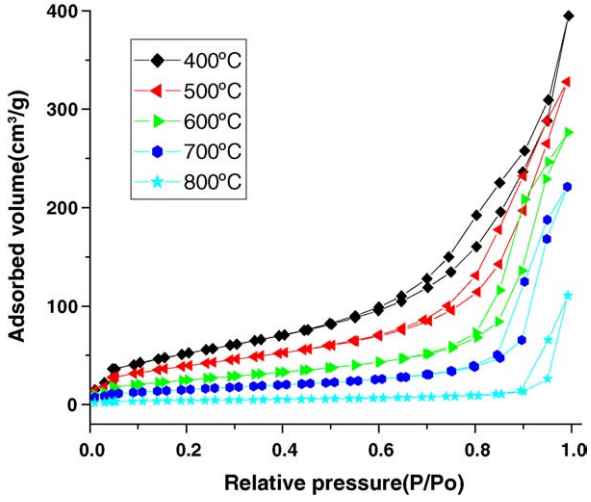

Fig. 4. N_2 adsorption–desorption isotherms of the as-prepared TiO_2 powders calcined at different temperatures.

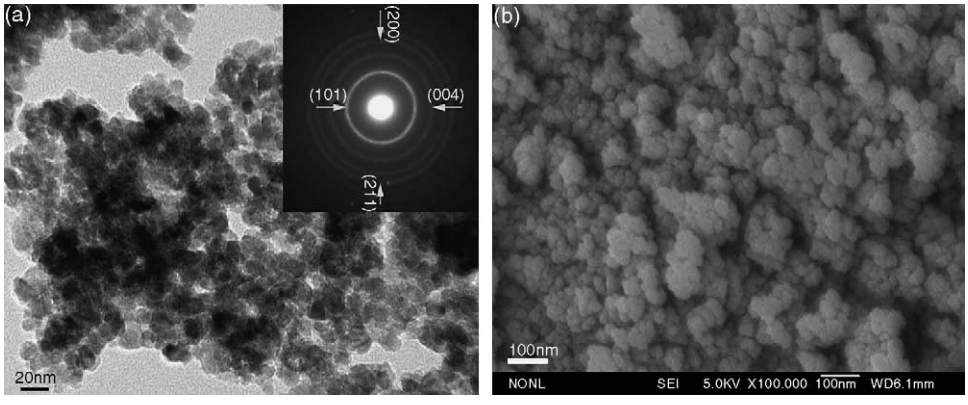

Fig. 3. (a) TEM image and SAED pattern (inset) and (b) SEM image of as-prepared TiO_2 calcined at 500 °C.

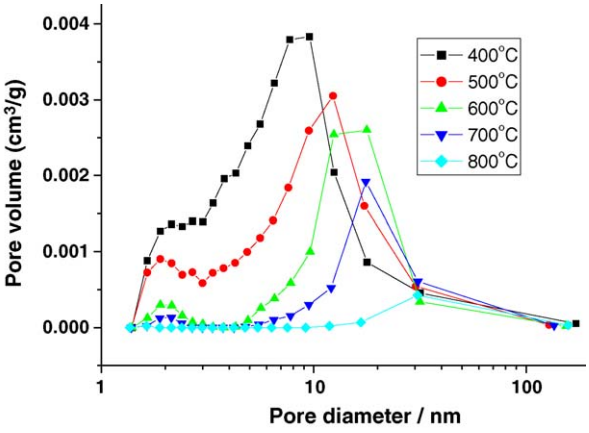

Fig. 5. Pore size distributions of the as-prepared TiO_2 powders calcined at different temperatures.

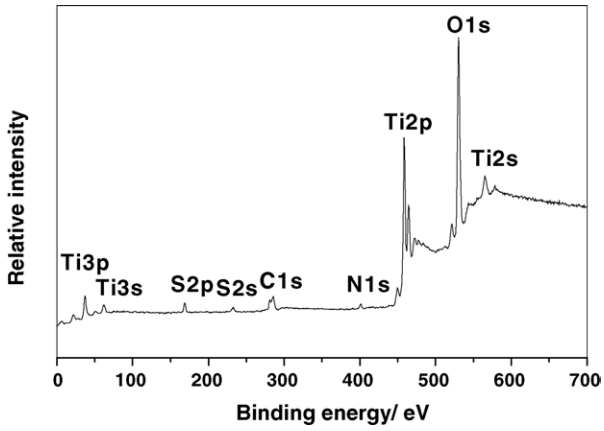

Fig. 6. XPS survey spectrum of the as-prepared TiO_2 powders calcined at 500 °C.

powders vary with increasing calcination temperatures. The isotherms of the TiO_2 powders calcined from 400 to 700 °C were a combination of types I and IV with two very distinct regions: at low relative pressure, the isotherm exhibited high adsorption, indicating that the powders contained micropores (type I). However, at high relative pressure between 0.6 and 1.0, the curve exhibited a hysteresis loop, indicating the presence of mesopores (type IV). At 800 °C, the isotherm of the TiO_2 powders belongs to type IV. With increasing calcination temperature, the hysteresis loops in the N_2 adsorption–desorption isotherms shifted to the region of higher relative pressure, and the areas of the hysteresis loops decrease. This indicated that the average pore size increased and the volume of pore decreased with increasing calcination temperatures [54]. Fig. 5 shows the pore size distribution of the TiO_2 powders calcined at different temperatures. All the powders except for the sample calcined at 800 °C show bimodal pore size distributions, that is, micropores with average pore diameters of 1.8 nm and mesopores with average pore diameters about 12.7–46.5 nm. The micropores may be resulted from intra-aggregated pores, while the mesopores may be assigned to the pores among inter-aggregated particles [54–56]. It can be seen that the diameter ranges of pores were located at 1.5–130 nm. With increasing calcination temperature, the average pore size increased from 12.7 to 46.5 nm. There were two factors resulting in the increase of pore size. One was that the smaller pores endured much greater stress than the bigger pores, so the small pores collapsed firstly during calcination. The other was that the bigger crystallites aggregation could form bigger pores. Therefore, the diameter of pore became bigger while the volume of pore became smaller with increasing calcination temperature.

Table 1 shows the effects of calcination temperature on the physical properties of the TiO_2 powders. It can be seen from Table 1 that TiO_2 powders calcined at 400 °C show a large specific surface area, pore volume and porosity, and their values reach 192.5 m^2/g, 0.611 cm^3/g and 70.5%, respectively. With increasing calcination temperature, the specific surface areas, pore volumes and porosity steadily decreased due to the growth of TiO_2 crystallite. At 800 °C, the specific surface area, pore volume and porosity of the TiO_2 powders decreased to 14.7 m^2/g, 0.171 cm^3/g and 40.0%, respectively. It is easy to note that all powders show a monotonic increase in the average pore size and the average crystalline size with increasing calcination temperature.

3.4. XPS analysis

Fig. 6 shows the XPS survey spectrum of the TiO_2 powders calcined at 500 °C. XPS survey spectrum shows that the TiO_2 powders contain not only Ti and O elements, but also a small amount of N, S and C elements. The following binding energies of elements are used in our quantitative measurements: Ti 2p at 458 eV, O 1s at 531 eV, N 1s at 400 eV, S 2p at 169 eV and C 1s at 285 eV. The atomic ratio of Ti:O:N:S is 1:2.03:0.04:0.03, which is in good agreement with the nominal atomic composition of TiO_2. The C element is ascribed to the adventitious hydrocarbons from the XPS instrument itself. The XPS spectra of other samples are similar.

Fig. 7(a) shows the high-resolution XPS spectra of the N 1s region, taken on the surface of TiO_2 powders. The N 1s region can be fitted into two peaks. The one is attributed to the Ti–N (binding energy is 400.4 eV) [33], which is probably formed by a nucleophilic substitution reaction between NH_3 and $Ti(SO_4)_2$ during the hydrolysis [11]. The other is probably assigned to some NH_3 adsorbed on the surface of TiO_2 [34,35]. It can be

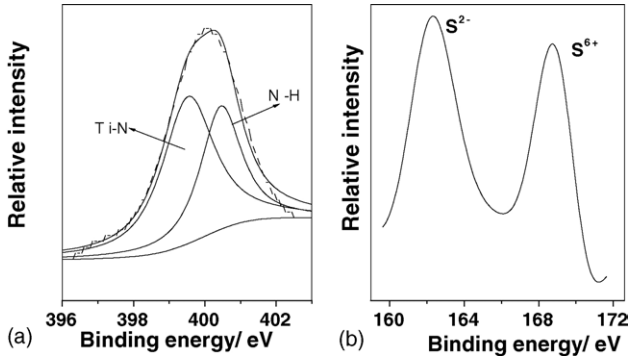

Fig. 7. High-resolution XPS spectra of N 1s (a) and S 2p (b) region of the as-prepared TiO_2 powders calcined at 500 °C.

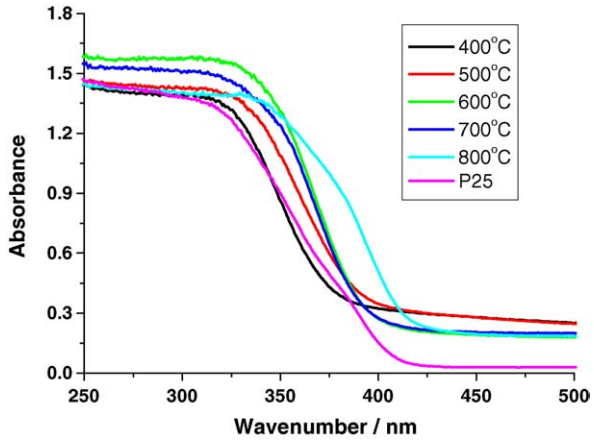

Fig. 8. UV–vis absorption spectra of the as-prepared TiO_2 powders calcined at different temperatures.

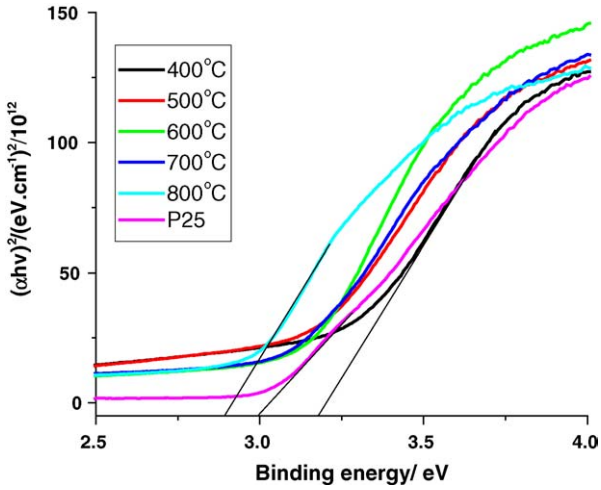

Fig. 9. Plots of the $(\alpha h\nu)^2$ vs. photon energy ($h\nu$) for the as-prepared TiO_2 powders calcined at different temperatures.

seen from Fig. 7(b) that the peak of S $2p_{3/2}$ contains two isolated peaks at binding energies of 168.7 and 162.3 eV, which can be attributed to the S (+VI) and S (−II), respectively. The S (+VI) may be assigned to the SO_4^{2-} ions adsorbed on the surface of TiO_2 powders. The peak at 162.3 eV corresponds to the Ti–S bond due to the fact that S atoms replaced O atoms in the TiO_2 lattice [36]. It can be reasonable to deduce that if the S^{2-} ions replace the O^{2-} ions in the lattice of TiO_2, a lattice distort may be created due to a large ionic radius difference between S^{2-} (1.7 Å) and O^{2-} (1.22 Å) [39]. XRD results further confirm the above deduction. The cell parameters a and c (calculated according to XRD result) of the N,S-codoped TiO_2 powders calcined at 500 °C were 3.785 and 9.512 Å, respectively [57], which were slightly bigger than those of pure anatase TiO_2 (JPCDS Card: 86–1157, a = 3.783 Å, c = 9.497 Å, space group:$I4_1/amd$). According to the above XPS results, it can be inferred that N and S elements were in situ codoped into TiO_2 during hydrolysis of $Ti(SO_4)_2$ in a $NH_3{\cdot}H_2O$ solution, and the N and S elements came from $Ti(SO_4)_2$ and $NH_3{\cdot}H_2O$, respectively.

3.5. UV–vis diffuse reflectance spectra

Usually, anions doping obviously affects light absorption characteristics of TiO_2 [19–21,28,29]. Fig. 8 shows the UV–vis absorption spectra of the N,S-codoped TiO_2 and Degussa P25 powders. A significant increase in the absorption at wavelengths shorter than 400 nm can be assigned to the intrinsic band gap absorption of TiO_2. The absorption spectra of the N,S-codoped TiO_2 samples show a stronger absorption in the UV–vis light region and a red shift in the band gap transition. Generally, the photocatalytic activity is proportional to $(I_\alpha\phi)^n$ (n = 1 for low light intensity and n = 1/2 for high light intensity), where I_α is the photo numbers absorbed by photocatalyst per second and ϕ is the efficiency of the band gap transition. The enhancement of the photoactivity with N,S-codoping can be partly explained in terms of an increase in $I_\alpha\phi$ resulting from intensive absorbance in the UV region [2,11]. Moreover, N and S codoping also expand the wavelength response range of TiO_2 into the visible region and increased the number of photo-generated electrons and holes to participate in the photocatalytic reaction. All these would enhance the photocatalytic activity of the N,S-codoped TiO_2 powders.

The red shift is ascribed to the fact that N,S-codoping can narrow the bad gap of the TiO_2. Further observation shows that the absorbance increases with increasing calcination temperature. At 400 °C, the absorbance of N,S-codoped TiO_2 in the UV region is similar to that of P25 and the absorbance in the visible region is higher than that of P25. At 500 °C, the absorbance of N,S-codoped TiO_2 is obviously higher than that of P25 in the whole UV–vis light region. This may be attributed to the fact that the high-temperature calcination can induce N and S elements doped into the lattice of TiO_2, resulting in the narrowing of the band gap. Other groups also reported similar results. For example, Colussi and co-workers [32] and Hashimoto and coworkers [56] prepared N-doped TiO_2 with visible-light activity by treating commercial anatase TiO_2 powders at 550 °C under a NH_3 flow for 3 h. Li et al. [37,38] synthesized N,F-codoped TiO_2 via spray pyrolysis method above 500 °C. Yu et al. [36] also fabricated S-doped TiO_2 by calcination in air at 500 °C for 1 h. At 800 °C, the N,S-codoped TiO_2 powders show a greatest red shift in the band gap transition due to the formation of rutile phase and growth of TiO_2 crystallite.

The absorption edge shifts toward longer wavelengths for the N,S-codoped TiO_2 powders. This clearly indicates a decrease in the band gap energy of TiO_2. The direct band gap energy can be estimated from a plot of $(\alpha h\nu)^2$ versus photon energy ($h\nu$). The intercept of the tangent to the plot will give a good approximation of the band gap energy for TiO_2 [15,58,59]. The absorption coefficient α can be calculated from the measured absorbance (A) according to the following equation [11],

$$\alpha = \frac{2.303\rho 10^3}{lcM}A \tag{6}$$

where the density ρ = 3.90 g cm^{-3}, molecular weight M = 80.0 g mol^{-1}, c the molar concentration of TiO_2 and l is the optical path length. Plots of the $(\alpha h\nu)^2$ versus photon energy ($h\nu$) are shown in Fig. 9. The direct band gap energies

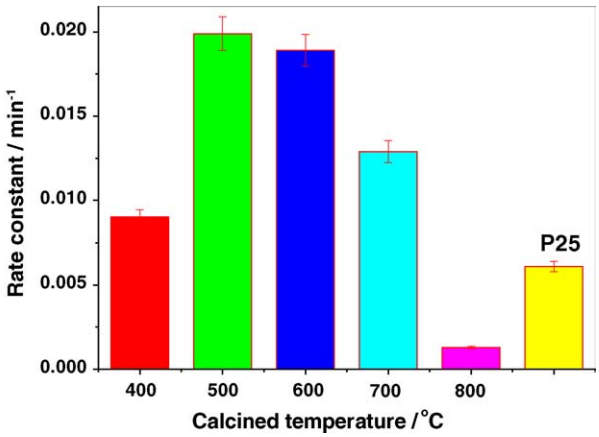

Fig. 10. The dependence of the apparent rate constants (k, min^{-1}) of photocatalytic oxidation of acetone under UV irradiation on calcination temperature.

estimated from the intercept of the tangents to the plots are 3.18, 3.08, 3.05, 2.98 and 2.90 eV for the N,S-codoped TiO_2 samples calcined at 400, 500, 600, 700 and 800 °C, respectively. The direct band gap energy of P25 is 3.00 eV. Therefore, it is not surprising that the direct band gap energy of the as-prepared powders is lower than that of anatase TiO_2 (pH 1, 3.20 eV) due to N,S-codoping.

3.6. Photocatalytic activity

The photocatalytic activity of the as-prepared TiO_2 powders was evaluated by the photodegradation of acetone or formaldehyde in air. However, under dark conditions without light illumination, the content of formaldehyde or acetone does not change for every measurement using various the as-prepared TiO_2 powders. Illumination in the absence of TiO_2 powders does not result in the photocatalytic reaction. Therefore, the presence of both illumination and TiO_2 powders is necessary for the efficient degradation. These results also suggest that the photocatalytic degradation of acetone or formaldehyde was caused by photocatalytic oxidation reactions on the surface of TiO_2 powders under the light illumination.

Many studies have shown that calcination is an effective treatment method to enhance the photoactivity and crystallization of nanosized TiO_2 photocatalysts [32,60–63]. Fig. 10 shows the dependence of the apparent rate constants (k, min^{-1}) for photocatalytic oxidation of acetone under UV irradiation on calcination temperature. All samples were prepared by hydrolysis of $Ti(SO_4)_2$ in a $NH_3{\cdot}H_2O$ aqueous solution. There is no photocatalytic activity observed when the calcination temperature is below 400 °C, which is due to the fact that the TiO_2 powders are composed of amorphous TiO_2. The sample calcined at 400 °C shows decent photocatalytic activity with a rate constant of 9.0×10^{-3}. This is due to the formation of anatase phase. The rate constant increases with increasing calcination temperature. The enhancement of photocatalytic activity at elevated temperatures can be ascribed to an obvious improvement in relative anatase crystallinity (as shown in Table 1). At 500 °C, the k reaches the highest value of 2.0×10^{-2}. This rate constant is significantly higher than that of P25 ($k = 6.1 \times 10^{-3}$), which is recognized as an excellent photocatalyst [2,63]. The high photocatalytic activity of the 500 °C sample is partially due to its large surface area, small crystallite size and good crystallization (as shown in Table 1). The specific surface area and crystallite size of P25 are about 63.0 m^2/g and 30 nm, respectively. Moreover, the intense absorption in the UV–vis light region and a red shift in the band gap transition of the N,S-codoped TiO_2 samples indicated that more photo-generated electrons and holes can participate in the photocatalytic reactions. Similar results have been also observed for the nitrogen and fluorine ions doping of TiO_2 [11,64–66]. It is well known that titania has three different crystalline phase: anatase, rutile and brookite, and the rutile has the lowest photocatalytic activity. The decrease in the phtotcatalytic activity of the N,S-codoped TiO_2 powders calcined at above 600 °C is due to the following factors. First, according to XRD results, the phase transformation of anatase to rutile occurred at about 700 °C. At 800 °C, the TiO_2 powders are mainly composed of rutile. Second, the sintering and growth of TiO_2 crystallites result in the significant decrease of surface area of the TiO_2 powders (as shown in Table 1). Also, the phase transformation from anatase to rutile further accelerates the growth of crystallites by providing the heat of phase transformation [53]. These causes may result in the rapid decrease of photocatalytic activity.

To further evaluate the photocatalytic properties of the as-prepared TiO_2 powders, the photodegradation of formaldehyde under daylight irradiation was also investigated. Fig. 11 shows the dependence of the removal efficiency (R(%)) of photocatalytic oxidation of formaldehyde under daylight irradiation on calcination temperature. At 400 °C, The sample shows high photocatalytic activity for photocatalytic oxidation of formaldehyde under daylight irradiation. With increasing calcination temperature, the removal efficiency (R) increased. At 500 °C, the photocatalytic activity of the powders reached a maximum value of R(%) = 64.0%. The value of R(%) is more than 10 times higher than that of P25 (R(%) = 5.0%). At a higher temperature, the removal efficiencies steadily decreased and reached a minimum value of 2.0% at 800 °C. This result further confirmed that the sample calcined at 500 °C possessed the highest photo-

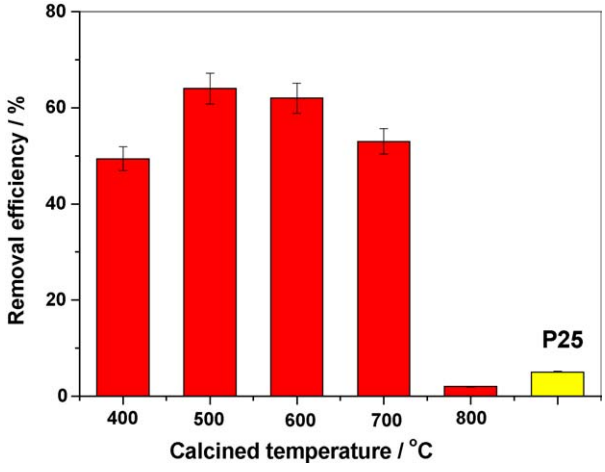

Fig. 11. The dependence of the removal efficiency (R(%)) of photocatalytic oxidation of formaldehyde under daylight irradiation on calcination temperature.

catalytic activity. It can be seen from the above results that the TiO_2 powders showed similar photocatalytic activities for photodegradation of both formaldehyde and acetone. The visible-light activity of the N,S-codoped TiO_2 may be caused due to band gap narrowing by mixing the N 2p and S 3p states with O 2p states, respectively. Hashimoto and co-workers [56,67] provided an alternative explanation that a localized N 2p state formed above the valence band was the origin for the visible-light activity of the nitrogen-doped TiO_2. Yu et al. [36] found that sulfur doping can indeed create intra-band gap states close to the conduction band edges, and thus induces visible-light absorption at the sub-band gap energy. Apart from band gap narrowing of the N,S-codoped TiO_2 powders, the constitution of the TiO_2 (doped and undoped TiO_2) also pay an important role in its high photoactivity. Usually, the composite of two kinds of semiconductors or two phases of the same semiconductor is beneficial in reducing the recombination of photo-generated electrons and holes, and thus enhances photocatalytic activity [41]. The interface between the two phases may act as a rapid separation site for the photo-generated electrons and holes due to the difference in the energy level of their conduction bands and valence bands. Therefore, the N,S-codoped TiO_2 powders prepared by hydrolysis method exhibit a significant photoactivity under daylight illumination due to the fact that the as-prepared TiO_2 powders consist of two phases of undoped TiO_2 and N,S-codoped TiO_2.

4. Conclusion

1. Highly active nanocrystalline mesoporous N,S-codoped TiO_2 photocatalysts were successfully prepared by a in situ wet chemical method. The photocatalytic activities of the as-prepared N,S-codoped TiO_2 powders calcined at a temperature range of 400–700 °C are obviously higher than that of commercial Degussa P25.
2. The N,S-codoped TiO_2 powders showed a stronger absorption in the UV–vis light region and a red shift in the band gap transition due to the fact that the band gap of N,S-codoped TiO_2 powders were narrowed by mixing the N 2p and S 3p states with O 2p states.
3. The daylight-induced photocatalytic activities of the as-prepared N,S-codoped TiO_2 powders were about ten times greater than that of Degussa P25. The high photoactivities of the as-prepared TiO_2 can be attributed to the results of the synergetic effects of strong absorption in the UV–vis light region, red shift in adsorption edge, good crystallization, large surface area and two phase structures of undoped TiO_2 and N,S-codoped TiO_2.

Acknowledgements

This work was partially supported by the National Science Foundation of China (50272049 and 20473059). This work was financially supported by the Excellent Young Teachers Program of MOE of China and Project-Sponsored by SRF for ROCS of SEM of China.

References

[1] M.A. Fox, M.T. Dulay, Chem. Rev. 93 (1993) 341.
[2] M.R. Hoffmann, S.T. Martin, W. Choi, D.W. Bahnemann, Chem. Rev. 95 (1995) 69.
[3] H. Tada, M. Yamamoto, S. Ito, Langmuir 15 (1999) 3699.
[4] A. Fujishima, T.N. Rao, D.A. Tryk, J. Photochem. Photobiol. C 1 (2000) 1.
[5] K. Nagaveni, G. Sivalingam, M.S. Hegde, G. Madras, Environ. Sci. Technol. 38 (2004) 1600.
[6] H. Einaga, T. Ibusuki, S. Futamura, Environ. Sci. Technol. 38 (2004) 285.
[7] P.V. Kamat, R. Huehn, R. Nicolaescu, J. Phys. Chem. B 106 (2002) 788.
[8] F.B. Li, X.Z. Li, M.F. Hou, Appl. Catal. B 48 (2004) 185.
[9] F.B. Li, X.Z. Li, Appl. Catal. A 228 (2002) 15.
[10] X.T. Hong, Z.P. Wang, W.M. Cai, F. Lu, J. Zhang, Y.Z. Yang, N. Ma, Y.J. Liu, Chem. Mater. 17 (2005) 1548.
[11] J.C. Yu, J.G. Yu, W.K. Ho, Z.T. Jiang, L.Z. Zhang, Chem. Mater. 14 (2002) 3808.
[12] J. Ovenstone, J. Mater. Sci. 36 (2001) 1325.
[13] E.C. Akubuiro, X.E. Verykios, J. Phys. Chem. Solids 50 (1989) 17.
[14] J. Soria, J.C. Conesa, V. Augugliaro, L. Palmisano, M. Schiavello, A. Sclafani, J. Phys. Chem. 95 (1991) 274.
[15] W. Choi, A. Termin, M.R. Hoffmann, J. Phys. Chem. 98 (1994) 13669.
[16] J. Moon, H. Takagi, Y. Fujishiro, M. Awano, J. Mater. Sci. 36 (2001) 949.
[17] J. Lin, J.C. Yu, D. Lo, S.K. Lam, J. Catal. 183 (1999) 368.
[18] Z.H. Yuan, J.H. Jia, L.D. Zhang, Mater. Chem. Phys. 73 (2002) 323.
[19] A. Hattori, K. Shimoda, H. Tada, S. Ito, Langmuir 15 (1999) 5422.
[20] J.S. Park, W. Choi, Langmuir 20 (2004) 11523.
[21] R. Asahi, T. Morikawa, T. Okwaki, K. Aoki, Y. Taga, Science 293 (2001) 269.
[22] T. Umebayashi, T. Yamaki, H. Itoh, K. Asai, Appl. Phys. Lett. 81 (2002) 454.
[23] T. Umebayashi, T. Yamaki, S. Tanala, K. Asai, Chem. Lett. 32 (2003) 330.
[24] T. Umebayashi, T. Yamaki, S. Yamamoto, A. Miyashita, S. Tanala, T. Sumita, K. Asai, J. Appl. Phys. 93 (2003) 5156.
[25] T. Ohno, T. Mitsui, M. Matsumura, Chem. Lett. 32 (2003) 364.
[26] T. Ohno, M. Akiyoshi, T. Umebayashi, K. Asai, T. Mitsui, M. Matsumura, Appl. Catal. A 265 (2004) 115.
[27] T. Ohno, Water Sci. Technol. 49 (2004) 159.
[28] W. Zhao, W. Ma, C. Chen, J. Zhao, Z. Shuai, J. Am. Chem. Soc. 126 (2004) 4782.
[29] T. Tachikawa, S. Tojo, K. Kawai, M. Endo, M. Fujitsuka, T. Ohno, K. Nishijima, Z. Miyamoto, T. Majima, J. Phys. Chem. B 108 (2004) 19299.
[30] J.G. Yu, J.C. Yu, B. Cheng, S.K. Hark, K. Iu, J. Solid State Chem. 174 (2003) 372.
[31] J. Premkumar, Chem. Mater. 16 (2004) 3980.
[32] M. Mrowetz, W. Balcerski, A.J. Colussi, M.R. Hoffmann, J. Phys. Chem. B 108 (2004) 17269.
[33] S. Sakthivel, M. Janczarek, H. Kisch, J. Phys. Chem. B 108 (2004) 19384.
[34] O. Diwald, T.L. Thompson, E. Zubkov, E.G. Goralski, S.D. Walck Jr, J.T. Yates, J. Phys. Chem. B 108 (2004) 6004.
[35] R. Nakamura, T. Tanaka, Y. Nakato, J. Phys. Chem. B 108 (2004) 10617.
[36] J.C. Yu, W.K. Ho, J.G. Yu, H. Yip, P.K. Wong, J.C. Zhao, Environ. Sci. Technol. 39 (2005) 1175.
[37] D. Li, H. Haneda, S. Hishita, N. Ohashi, Chem. Mater. 17 (2005) 2588.
[38] D. Li, H. Haneda, S. Hishita, N. Ohashi, Chem. Mater. 17 (2005) 2596.
[39] R. Bacsa, J. Kiwi, T. Ohno, P. Albers, V. Nadtochenko, J. Phys. Chem. B 109 (2005) 5994.
[40] J.M. Mwabora, T. Lindgren, E. Avendano, T. Jaramillo, J. Lu, S.E. Lindquist, C.G. Granqvist, J. Phys. Chem. B 108 (2004) 20193.
[41] J.C. Yu, J.G. Yu, W.K. Ho, L.Z. Zhang, Chem. Commun. (2001) 1942.

[42] H. Zhang, J.F. Banfield, J. Phys. Chem. B 104 (2000) 3481.
[43] C.Y. Wang, C. Bottcher, D.W. Bahnemann, J.K. Dohrmann, J. Mater. Chem. 13 (2003) 2322.
[44] S. Ito, S. Inoue, H. Kawada, H. Hara, M. Iwasaki, H. Tada, J. Colloid Interface Sci. 216 (1999) 59.
[45] K.S.W. Sing, D.H. Everett, R.A.W. Haul, L. Moscou, R.A. Pierotti, J. Rouquerol, T. Siemieniewska, Pure Appl. Chem. 57 (1985) 603.
[46] J.G. Yu, M.H. Zhou, B. Cheng, H.G. Yu, X.J. Zhao, J. Mol. Catal. A 227 (2005) 75.
[47] M.H. Zhou, J.G. Yu, B. Cheng, H.G. Yu, Mater. Chem. Phys. 93 (2005) 159.
[48] J.C. Yu, J.G. Yu, J.C. Zhao, Appl. Catal. B 36 (2002) 31.
[49] A. Fernandez, G. Lassaletta, V.M. Jimenez, A. Justo, A.R. Gonzalez-Elipe, J.M. Herrmann, H. Tahiri, Y. Ait-Ichou, Appl. Catal. B 7 (1995) 49.
[50] J.G. Yu, X.J. Zhao, Q.N. Zhao, Thin Solid Films 379 (2000) 7.
[51] K. Terabe, K. Kato, H. Miyazaki, S. Yamaguchi, A. Imai, Y. Iguchi, J. Mater. Sci. 29 (1994) 1617.
[52] J.G. Yu, J.C. Yu, W.K. Ho, M.K.P. Leung, B. Cheng, G.K. Zhang, X.J. Zhao, Appl. Catal. A 255 (2003) 309.
[53] J.G. Yu, H.G. Yu, B. Cheng, X.J. Zhao, J.C. Yu, W.K. Ho, J. Phys. Chem. B 107 (2003) 13871.
[54] J.G. Yu, J.C. Yu, M.K.P. Leung, W.K. Ho, B. Cheng, X.J. Zhao, J.C. Zhao, J. Catal. 217 (2003) 69.
[55] C. Kormann, D.W. Bahnemann, M.R. Hoffman, J. Phys. Chem. 92 (1988) 5196.
[56] H. Irie, S. Washizuka, N. Yoshino, K. Hashimoto, Chem. Commun. (2003) 1298.
[57] W. Huang, X. Tang, Y. Wang, Y. Koltypin, A. Gedanken, Chem. Commun. 15 (2000) 1415.
[58] J.A. Wang, R.L. Ballesteros, T. Lopez, A. Moreno, R. Gomez, O. Novaro, X. Bokhimi, J. Phys. Chem. B 105 (2001) 9692.
[59] G. Rothenberger, J. Moser, M. Graetzel, N. Serpone, D.K. Sharma, J. Am. Chem. Soc. 107 (1985) 8054.
[60] P.G.F. Bisling, E. Ruhl, B. Brutschy, H. Baumgartel, J. Phys. Chem. 91 (1987) 4310.
[61] H. Kominami, S. Murakami, M. Kohno, Y. Kera, K. Okada, B. Ohtani, Phys. Chem. Chem. Phys. 3 (2001) 4102.
[62] Y. Tanaka, M. Suganuma, J. Sol–Gel Sci. Technol. 22 (2001) 83.
[63] K.Y. Jung, S.B. Park, Korean J. Chem. Eng. 18 (2001) 879.
[64] J.C. Yu, J. Lin, D. Lo, S.K. Lam, Langmuir 16 (2000) 7304.
[65] A. Piscopo, D. Robert, J.V. Weber, J. Photochem. Photobiol. A 139 (2001) 253.
[66] T. Morikawa, R. Asahi, T. Okwaki, K. Aoki, Y. Taga, Jpn. Appl. Phys. Lett. 132 (2000) 99.
[67] H. Irie, Y. Watanabe, K. Hashimoto, J. Phys. Chem. B 107 (2003) 5483.